Gas Separations with Polymer Membranes

D. V. Laciak and M. Langsam, Corporate Science and Technology Center, Air Products and Chemicals Inc., Allentown, PA, USA

Introduction

In 1996 the worldwide industrial gas market was in excess of \$29 billion (US). It continues to grow at an average rate of 4–5% per annum. Industrial gases account for some of the largest production volume chemicals (1998 US): nitrogen (843 bcf (billion cubic feet)), oxygen (698 bcf) and ammonia (19 700 million tons). Oxygen and nitrogen are separated from purified air. Ammonia is produced by the reaction of nitrogen and hydrogen. Certainly, the vast majority of industrial gases are purified using cryogenic distillation or adsorption technology. However, in the last 20 years there has been a growing interest in and an intense effort on the part of major gas producers to evaluate and develop membrane technology to produce or purify gases. By 1999 sales of gas separation membrane technology exceeded \$100 million per year. This article will describe basic concepts along with various practical aspects of polymeric gas separation membranes including permeability measurement, membrane formation, module fabrication and applications.

A polymeric membrane is defined as a thin, semipermeable barrier between two gaseous phases. Gases will permeate the membrane if a difference in their chemical potential exists between the two gaseous phases. The chemical potential difference is most often a result of pressure differences across the membrane. Thus, gases will solubilize into the membrane at the high pressure interface, diffuse across the membrane in a concentration gradient to the low pressure interface and evolve into the low pressure gas phase (**Figure 1**). If a mixture of gases comprised of components i and j is brought into contact with the membrane, the permeate stream will be enriched in the more permeable gas i, leaving the retentate enriched in gas j.

The realization that gases permeate through polymers is not new. Every child knows that a balloon filled with air or helium deflates over time. Indeed, this phenomenon was observed by Mitchell in 1831. Balloons made of natural rubber filled at different rates depending on the gaseous atmosphere they were placed into. Carbon dioxide filled the balloon fastest, air slowest. Thirty-five years later Graham expanded

on Mitchell's experiments and quantitatively measured the permeation rates of gases through natural rubber. He found that the permeation rate was not related to the known *gaseous* diffusion coefficients and so concluded that permeation does not proceed through microscopic pores in the rubber but must occur within the rubber itself. He also demonstrated that natural rubber could be used to produce from air a permeate which was enriched in oxygen to 46%.

A mathematical description of the permeation process was proposed by Fick. The relationship between permeation rate J, gas pressure P, membrane area A and membrane thickness l, known as Fick's first law, is governed by eqn [1], where ΔP is the pressure difference across the membrane:

$$J = P_o \cdot A \cdot \Delta P / l \qquad [1]$$

The proportionality constant, P_o, is termed the permeability:

$$P_o = \frac{J \cdot l}{A \cdot \Delta P} = \frac{\text{volume gas} \cdot \text{thickness}}{\text{area} \cdot \text{time} \cdot \Delta P} \qquad [2]$$

The customary unit of permeability is the barrer where:

$$1 \text{ barrer} = 10^{-10} \frac{\text{cm}^3 \cdot \text{cm}}{\text{cm}^2 \cdot \text{s} \cdot \text{cmHg}} \qquad [3]$$

Permeability can also be written as the product of the gas solubility times its diffusivity, the so-called *solution–diffusion* mechanism (eqn [4]). The permselectivity (α) for two gases i and j is defined as the ratio of the permeabilities:

$$P_o = D \cdot S \qquad [4]$$

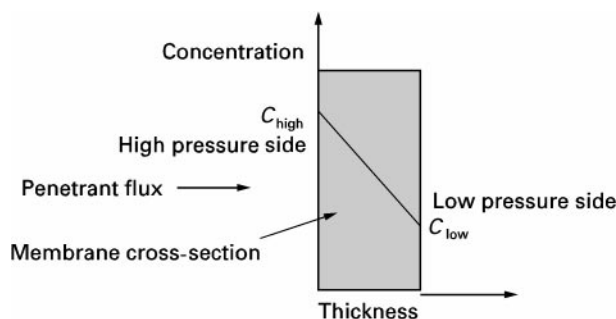$$\alpha_{ij} = P_{o_i} / P_{o_j} \qquad [5]$$

Figure 1 Schematic representation of membrane permeation.

Permeation is an activated process. The effect of temperature on permeation is given by eqn [6], where E_p is the activation energy of permeation, R is the gas constant and T is temperature:

$$P_o = P'_o \cdot \exp(-E_p/RT) \qquad [6]$$

In typically encountered cases E_p is postive and the permeability increases exponentially with temperature. Additionally, E_p is related to penetrant size and therefore selectivity usually decreases with increasing temperature. This treatment is not true when dealing with gases below their critical temperature. The reader is referred to the Further Reading section for these special cases.

The above equations give a mathematical, phenomenological description of gas permeation through polymers but imply nothing of the molecular-level processes giving rise to permeation. While we speak of gas-separating polymers as being dense films, on a molecular level one must consider that the membrane is not 'solid'; that is, there are molecular-size gaps between the polymer chains. These gaps arise from packing defects in the solid state and also arise from the thermal motions of the polymer chains themselves. It is through pemanent and transient gaps that gas transport is believed to occur. Solution-diffusion behaviour has proven adequate to describe permeation through rubbery polymers – those whose glass transition temperature, T_g, is below the experimental temperature. As a family, rubbery materials are highly permeable but unselective for the same molecular-level rationalization. In the rubbery state polymer chains are highly mobile, generating a high frequency of transient gaps which the penetrant gases can easily diffuse through. However, these gaps are not very selective. From a practical perspective, the purity of the product is related to the membrane permselectivity. With some exceptions, such as the
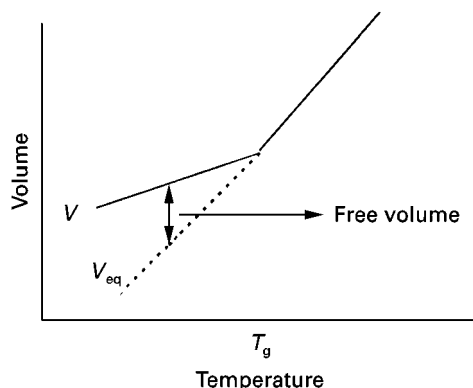
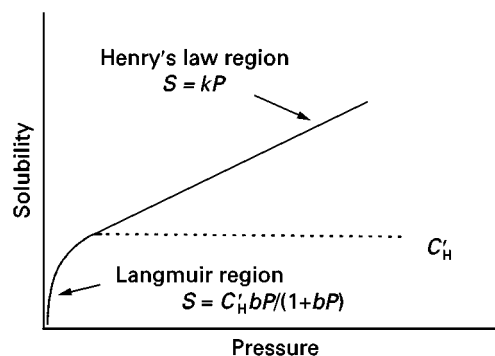production of oxygen-enriched air for medical applications or the recovery of C4 hydrocarbons, low-selectivity membranes and hence rubbery polymers have found limited commercial utility in the purification of industrial gases.

Dual-Mode Permeation in Glassy Polymers

Polymers in the glassy state possess 'free volume' as shown in Figure 2 – that is, a polymer quenched below its T_g to a nonequilibrium state in which its molar volume is higher than the equilibrium value. This free volume can be visualized as long-lived molecular-level gaps between the polymer chains. One aspect of free volume is that glassy polymers exhibit excess sorption capacity. Sorption in glassy polymers can be described by eqn [7]:
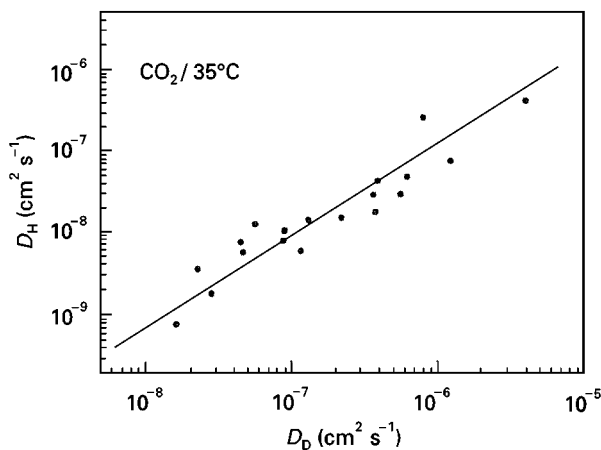
$$S = k_D P + \frac{C'_H bP}{1 + bP} \qquad [7]$$

Figure 3 Dual-mode sorption isotherm.

Figure 2 Schematic of free volume.

Figure 4 Coupling of Langmuir and Henry's mode diffusion coefficients.
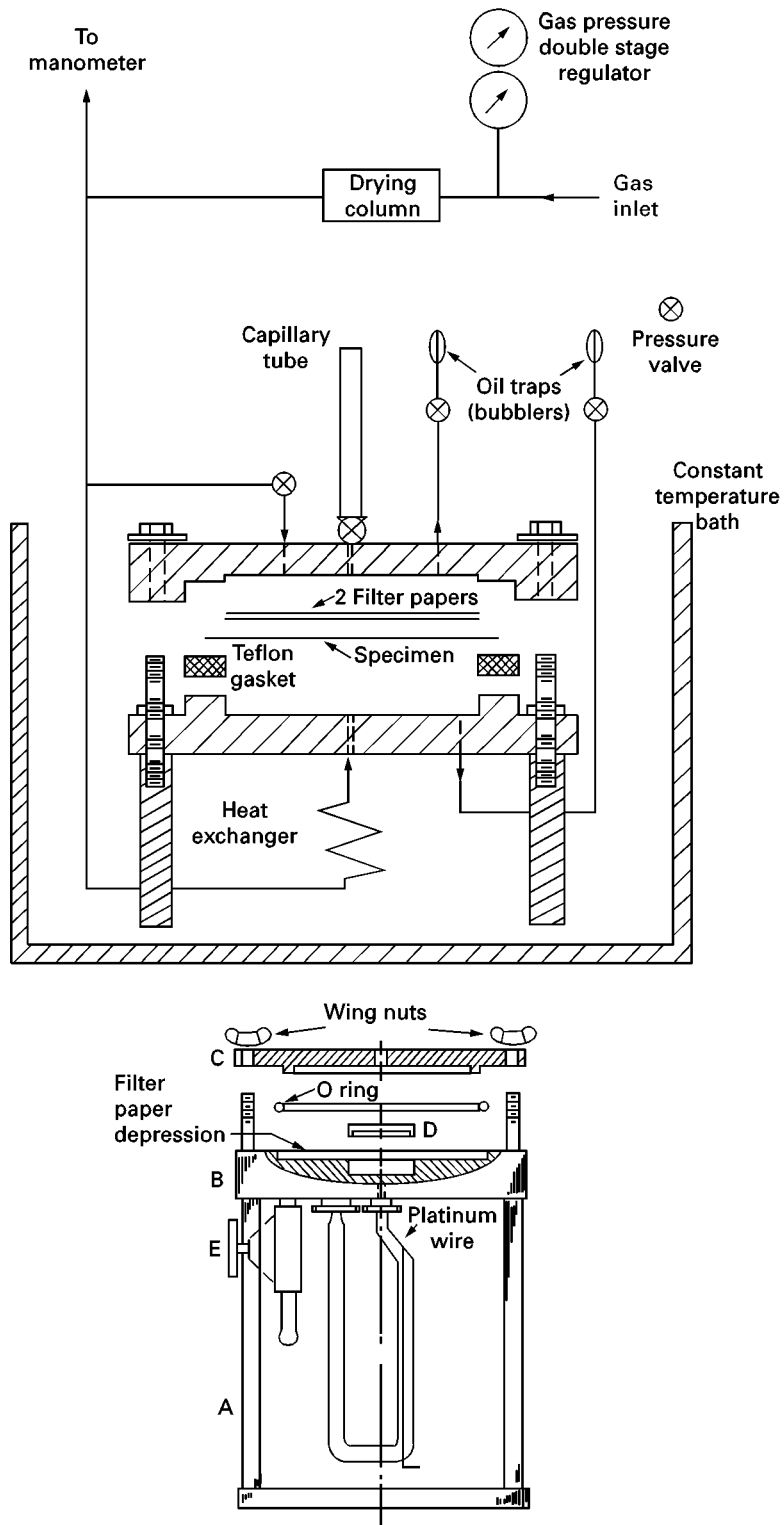
Figure 5 Permeability test cells. A, supporting legs; B, lower plate; C, upper plate; D, adapter; E, vacuum valve.

where k_D is the Henry's law solubility constant, b is the Langmuir equilibrium constant and C'_H is the Langmuir capacity and can be related to the free volume. Such sorption is often termed 'dual-mode' behavior. A typical dual-mode sorption isotherm is shown in **Figure 3**. At low pressures, sorption is dominated by the Langmuir element, while at high pressure sorption is described by Henry's law.
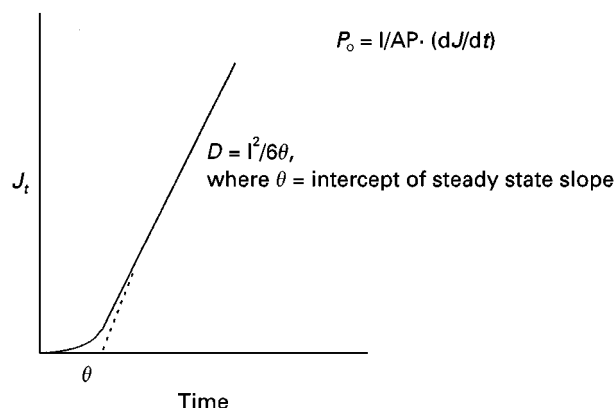
Figure 6 Time lag diffusion experiment.

Table 1 Air separation characteristics of some common polymers

Polymer	P_o O_2 (barrer)	α O_2/N_2
Polyacrylonitrile	0.0002	>10
Polyvinylidene chloride	0.0053	5.6
Polyethylene terephthalate	0.059	4.5
Cellulose acetate	0.78	2.8
Polystyrene	2.63	3.3
Poly(4-methyl-1-pentene)	32.3	4.1
Silicone rubber	610	2.0
Poly(trimethylsilylpropylene)	8000	1.4

Dual-mode permeation can be viewed as the simultaneous diffusion of gas molecules within and between the dense polymer phase and the Langmuir gaps or 'holes'. Dual-mode permeation then is described by the sum of permeation in these phases (eqn [8]). The two diffusion coefficients D_D and D_H appear to be strongly correlated to each other (**Figure 4**):

$$P_o = P_o \text{ (dense)} + P_o \text{ (hole)} = S_D D_D + S_H D_H$$

$$P_o = k_D D_D + \frac{C'_H b D_H}{1 + bP} \qquad [8]$$

Some consequences of dual-mode transport are:

1. The permeability of a dual-mode system decreases as the pressure is increased.

2. Condensible vapours such as water and higher hydrocarbons are strongly adsorbed in the high enthalpy free volume sites and deleteriously affect permeation rates and permselectivity.
3. Strongly absorbing gases such as CO_2 can swell the membrane at high pressure.
4. The free volume, a manifestation of the non-equilibrium state of the polymer, can be decreased by annealing or upon aging.

Methods of Measuring Permeability

Conceptually, measuring the gas permeability of polymeric membranes is simple although fraught with experimental pitfalls related to establishing steady state flow. The experimental parameters are given in eqn [2]. Several methods and apparatus have been developed to conduct permeability measurements. For obtaining the permeation pure gases one
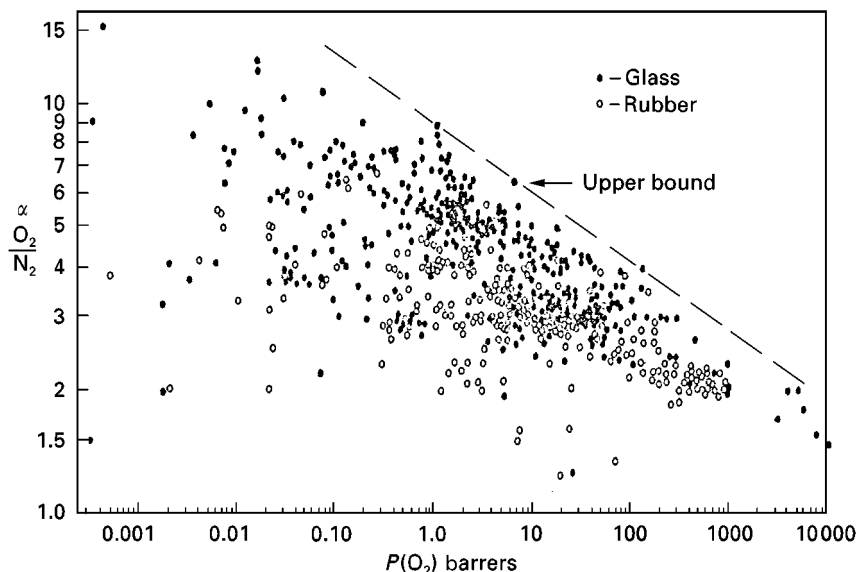

Figure 7 Upper bound representation of oxygen/nitrogen permselectivity – 1990.

Lennard–Jones kinetic diameters of various gases

Gas	He	H$_2$	CO$_2$	O$_2$	N$_2$	CH$_4$
Kinetic diameter (Å)	2.6	2.89	3.3	3.46	3.64	3.8

Table 2 Upper bound parameters

$$P_i = k\alpha_{ij}^n$$

Gas pair (ij)	k (barrer)	n
O$_2$/N$_2$	389 224	− 5.800
H$_2$/CH$_4$	18 500	− 1.2112
CO$_2$/CH$_4$	1 073 700	− 2.6264
He/N$_2$	12 500	− 1.0242
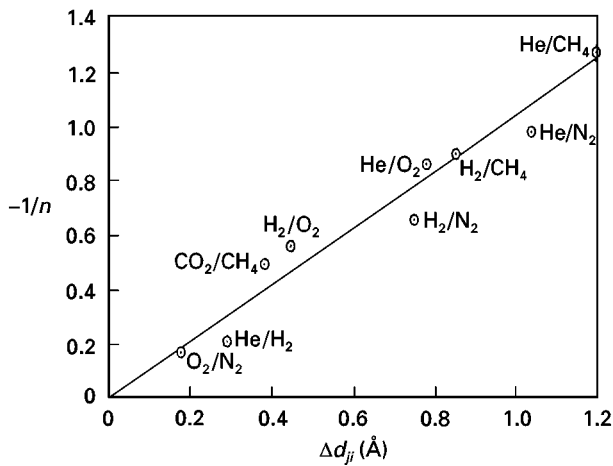
Figure 8 Relationship between the upper bound slope (n) and kinetic diameter difference of gas pairs ij.

measurers either the rate of permeability pressure rise (usually from a vacuum) in a constant volume/temperature receiver or the volume of permeate gas at a fixed pressure (**Figure 5**). Commercially available test cells are known as the volumetric or 'Linde cell' and the manometric or 'Dow' cell. The American Society of Testing and Materials has published a method for measuring gas permeability (ASTM Method D1434-82). It is possible to obtain the

permeability coefficient P_o and the diffusion coefficient D through a *time lag* measurement as shown in **Figure 6**; subsequent calculation of the solubility term though an independent measurement of S is advised.

Measuring the permeability of gas mixtures is more complex. Usually a flow of a pre-blended source is passed over the feed side of the membrane. The steady state permeate flux can be measured by employing an inert gas such as helium to sweep the permeating components into a gas chromatograph, for example, for compositional analysis. Preferably the experiment is conducted such that back-diffusion of the helium sweep is insignificant and where the feed gas composition is not altered by permeation. Additionally, nuances in the flow patterns within test cells not specifically designed for mixed gas experiments can lead to erroneous results.

Optimization of Polymer Permeation Properties

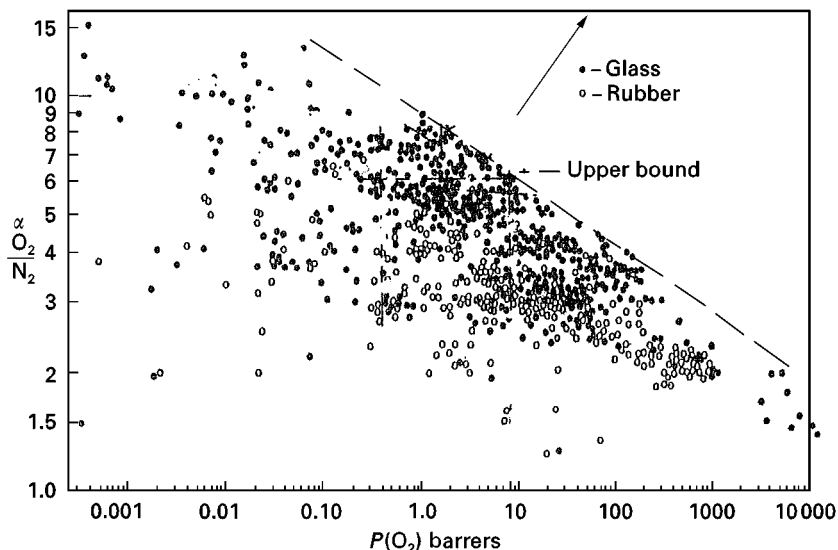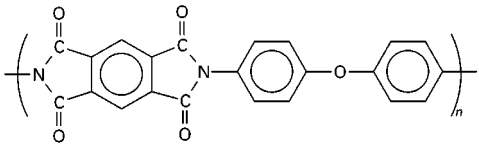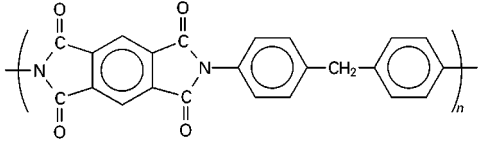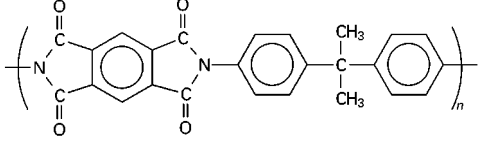**Table 1** illustrates the range of oxygen permeability and oxygen/nitrogen permselectivity for some
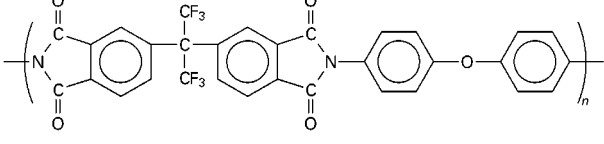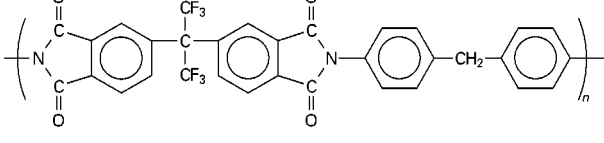
Figure 9 Upper bound representation of oxygen/nitrogen permselectivity – 1993.

Table 3 Structure–property relationships in polymer membranes

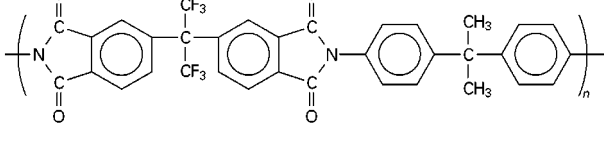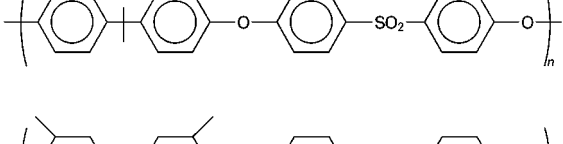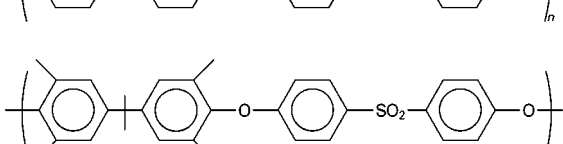| Polymer	Structure	Density (g cm^{-3})	d-spacing (Å)	P (O$_2$) (barrer)	O$_2$/N$_2$
PMDA-ODA		1.40	4.6	0.61	6.1
PMDA-mDA		1.35	4.9	0.98	4.9
PMDA-IPA		1.28	5.5	7.1	4.7
6FDA-ODA		1.43	5.6	3.9	5.34
6FDA-mDA		1.40	5.6	4.6	5.70
6FDA-IPA		1.35	5.7	7.5	5.60
PSF		1.24	5.0	1.4	5.60
DMPSF		1.21	5.0	0.64	7.00
TMPSF		1.15	5.5	5.6	5.28

common polymers. Permeability spans a wide range: seven orders of magnitude. Further, as the permeability of polymers increases, their ability to differentiate between gases, the permselectivity, decreases. This correlation is valid for nearly all polymeric membranes and has been the subject of research. While long recognized, this observation was first formalized by Robeson in 1991. Working with a database of over 200 polymers, the selectivity of several gas pairs, plotted on a log–log scale against the permeability of the faster gas, exhibits a characteristic upper bound defining the combinations of permeability and permselectivity simultaneously achievable with polymeric materials (**Figure 7**). Upper bound performance can be described by eqn [9]:

$$P_i = k\alpha_{ij}^n \quad or \quad \alpha_{ij} = k^{-1/n}P_i^{1/n} \qquad [9]$$

where the values of k and n, tabulated in **Table 2**, are calculated from the upper bound relationship for specific gas pairs. The parameter n is related to the difference in kinetic diameters of the penetrant gas pair Δd_{ij} as shown in **Figure 8**. This empirical treatment implies that the upper bound is a natural result of the sieving characteristic of stiff chain glassy polymers. A fundamental theory was later developed by Freeman in which the constants could be related to gas size and gas condensability and invoked just a single adjustable parameter f:

$$\ln \alpha_{ij} = -\lambda_{ij}\ln D_i + \{\ln(S_i/S_j) - \lambda_{ij}(b - f(1-a)/RT)\} \qquad [10]$$

where $\lambda_{ij} = [(d_i/d_j)^2 - 1]$ and d_i is the kinetic diameter; $S_i/S_j = N(\varepsilon_i/k - \varepsilon_j/k)$, where k is the Boltzmann constant and ε is the potential energy well depth in the Lennard–Jones potential energy function. The constants a and b are derived from linear free energy relationships and are independent of gas type. Moreover a is independent of polymer and has a universal value of 0.64; b has a value of 11.5 for glassy polymers and 9.2 for rubbery polymers. The solubility selectivity among polymers is largely constant; consequently diffusivity considerations dominate upper bound permselectivity.

The optimization of polymer structure to obtain upper bound properties comprises the lion's share of polymer membrane research in the last 20 years and the reader is referred to the Further Reading section. Researchers have heuristically developed the understanding gained via the upper bound analysis. The permselectivity for gases i and j is given by eqns [4] and [5] as:

$$\alpha_{ij} = Po_i/Po_j = (S_i/S_j) \cdot (D_i/D_j) \qquad [11]$$
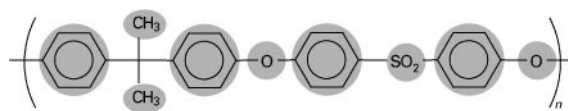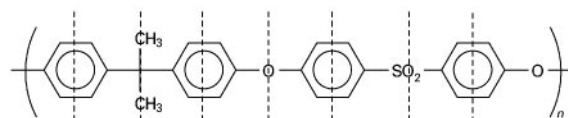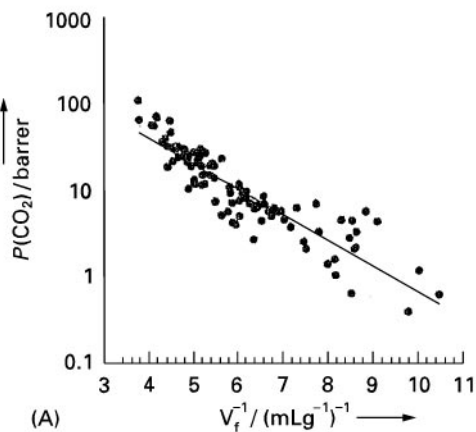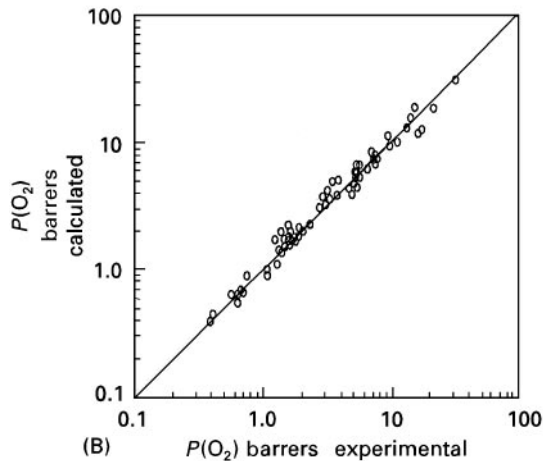
Figure 10 Structure–property relationship: (A) FFV model (Paul). (B) Robeson model.

The solubility selectivity (S_i/S_j) is nearly constant across a wide variety of polymers and for O_2/N_2 is about 2. Selectivity in glassy polymers is therefore dominated by the diffusive selectivity which in turn results from the sieving properties of the imperfectly packed polymer chains. The best trade-off in permeability properties within a polymer family is obtained when both main chain mobility is limited and intersegmental packing of polymer chains is

Figure 11   Structure units with imparting superior permselectivity.

Figure 12   Cross-section of an asymmetric membrane.

inhibited. This behaviour is illustrated (**Table 3**) for a family of pyromellitic dianhydride (PMDA) and hexafluoro-isopropylidene dianhydride (6FDA)-based polyimides.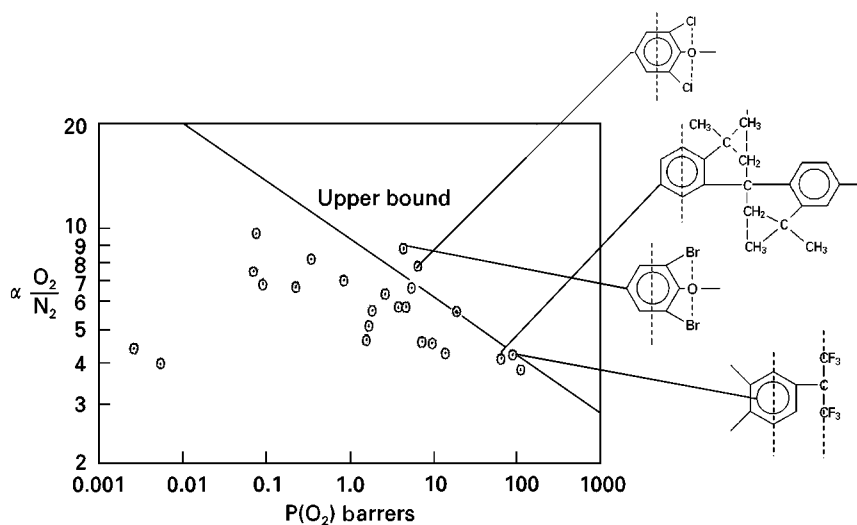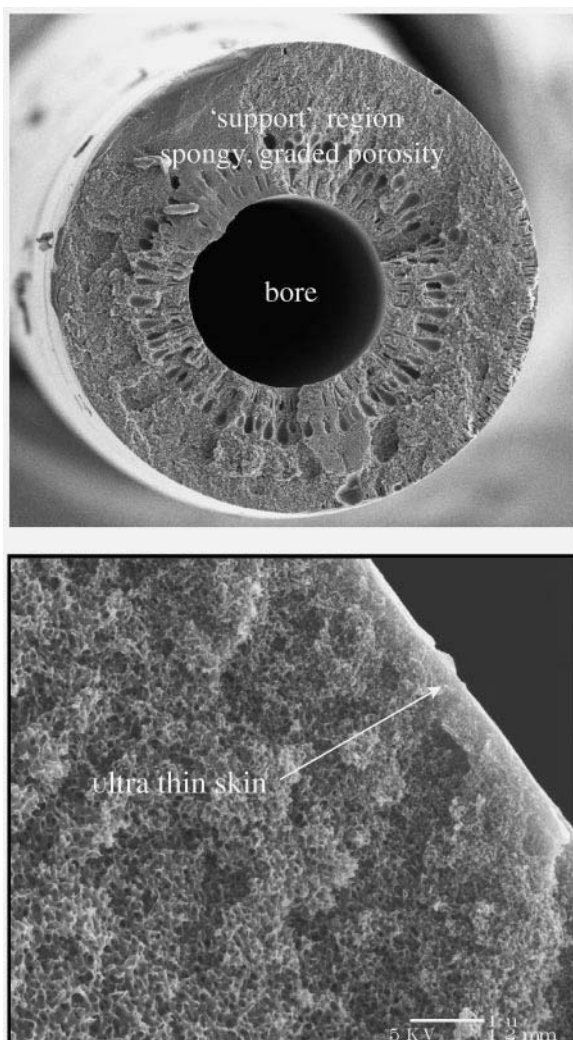 Changes in the functionality lead to different packing arrangements as measured by density and X-ray d-spacings (average distance between polymer chains). Very small changes in chain packing result in significant changes in both permeability and selectivity. Further, groups such as 6FDA are particularly desired because they can increase permeability without a large loss of selectivity. A further example is that of *ortho*, di- versus tetra-substitution patterns on aromatic polymers. It is widely recognized that incorporation of bulky substituents leads to an increase in permeability, usually at a loss of selectivity. However, it is also noted that *ortho* di-substitution patterns result in lower permeability and higher selectivity than the symmetrically tetra-substituted analogue. Using this intuitive approach a great many new polymers were synthesized and characterized between 1990 and 1993 and as a result the empirically determined upper bound has been shifted upwards and its slope has changed (**Figure 9**), with many polymers lying at or near the upper bound.

Predicting Polymer Permeability

The benefit of being able to predict *a priori* the relationship between polymer structure or physical properties and permeability is obvious. One method is to correlate the permeability with the reciprocal of the fractional free volume (FFV), defined as:

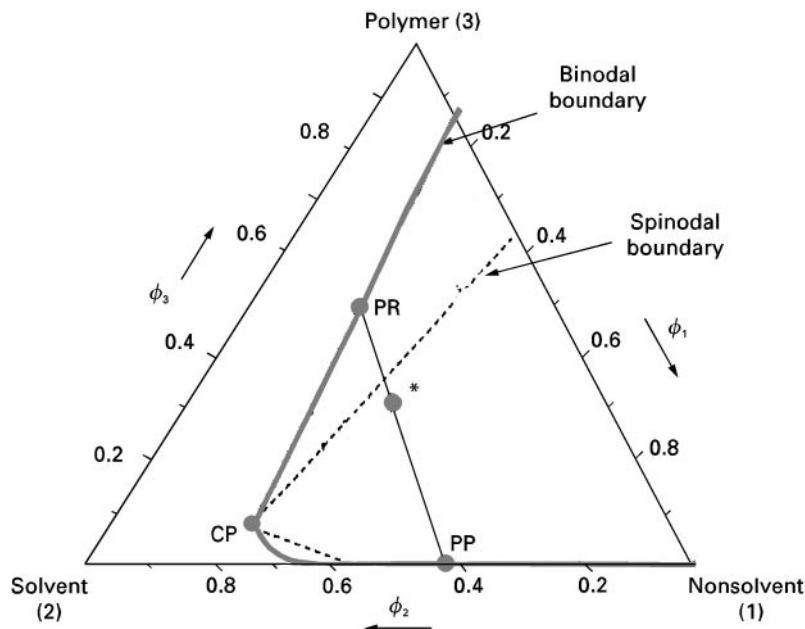$$FFV = \frac{V - V_o}{V} \qquad [12]$$

Figure 13 Phase diagram for a ternary dope system. PP, polymer-poor; PR, polymer-rich; CP, critical point.

where V is the specific volume of the polymer and V_o is the volume occupied by the polymer chains. The specific volume is obtained from experimental density measurement. Direct measurement of V_o is not possible and therefore various computational approaches have been developed. The most widely used is that developed by Bondi relating the zero point volume (the volume occupied at 0 K) to the van der Waals volume of the molecule and later modified by Park to account for the fact that different gases have access to different FFV depending on the specific gas–polymer interaction. This group contribution approach has yielded good correlations (**Figure 10A**) but it is not intuitively obvious how to relate polymer structure directly to free volume.

The group contribution approach by Robeson asserts that the overall polymer permeability can be represented by the sum of structural subunits that comprise the polymer in proportion to their volume fraction:

$$\ln P_o = \sum \phi_i \cdot P_i \qquad [13]$$

where ϕ_i is the volume fraction of subunit i and P_i its permeability contribution. Volume fractions are calculated using molecular mechanics computer modelling and the P_o's are experimentally determined. The P_i's are found by regressing the set of simultaneous linear equations from eqn [13]. In addition to adequately representing the experimental data (Figure 10B), this method also identifies those subunits which exhibit upper bound properties

(**Figure 11**). Desirable moieties include the 6FDA, di-*ortho* substituted phenyl ethers and the spirobiindane fragment. A superior polymer would be tetrabromo-poly(phenylene oxide); however, no one has as yet succeeded in its synthesis.

Membrane Formation

Most research on polymeric membrane materials is conducted on thin, solvent-cast, films. The practical limit to such membranes is about 25 μm for freestanding films and perhaps 1 μm if the polymer solution is cast on a microporous substrate. However, at these thicknesses the flux through the membrane is too low to be of practical value. That is to say, the economics of a membrane process utilizing these thick films would not effectively compete with established technologies such as cryogenic distillation. The enabling development for fabricating ultrathin, high flux membranes was the integrally skinned asymmetric membrane of Loeb and Sourirajan. This type of membrane is produced by inducing phase separation
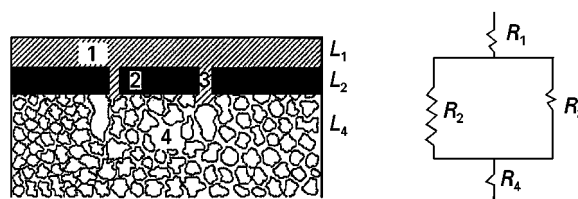
Figure 14 Series resistance model for defect repair.
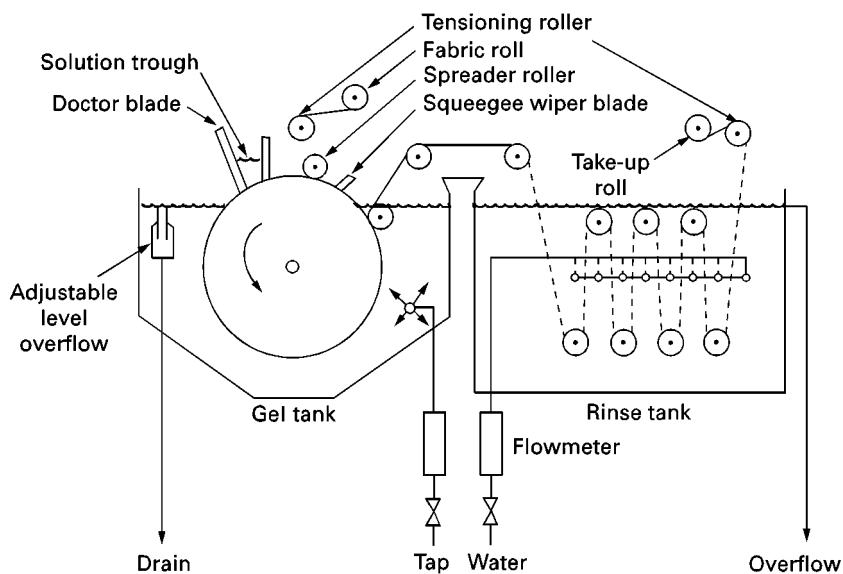
Figure 15 Flat-sheet membrane fabrication.

in a thermodynamically stable solution, usually by changing its composition through the introduction of a nonsolvent. These membranes are prepared by casting a concentrated polymer solution (dope) incorporating a water-miscible solvent into a water coagulation bath. Such membranes possess an ultrathin dense skin that gradually opens into a microporous substructure (**Figure 12**). The skin layer provides the

Figure 16 Spiral-wound membrane element.

separation while the thicker integral substructure provides robustness but very little resistance to gas flux.

Membrane formation processes can be grouped into three methods:

1. Dry phase inversion processes involve thermally quenching a dope or solvent evaporation in multi-component solvent system dopes.
2. Wet phase inversion processes involve quenching a cast dope in a coagulation bath.
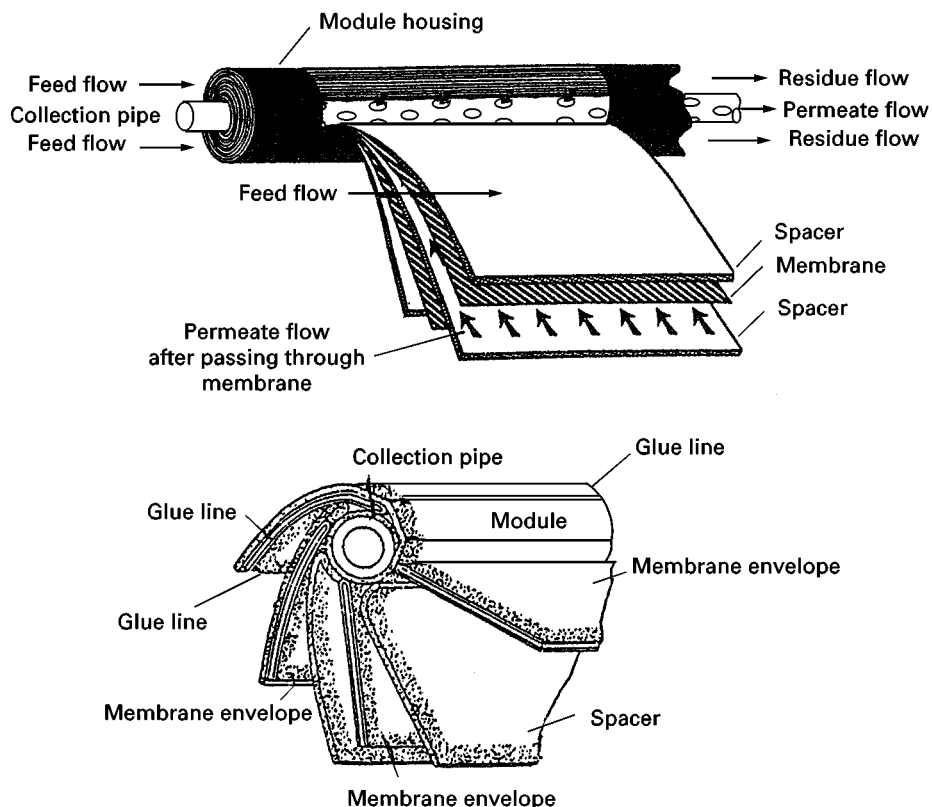3. Dry-wet phase inversion processes combine solvent evaporation and a quench medium.

Most commercial gas separation membranes are produced by the dry–wet process although temperature-induced phase inversion (TIPS) is also employed.

Phase diagrams illustrate the phase inversion process (**Figure 13**). The binodal defines the boundary of the two-phase region and is divided into two parts at the critical point (CP). A second envelope, the spinodal line, also emerges at the critical point. The phase inversion process involves bringing a dope solution into the two-phase envelope. The initially stable solution (at a composition designated by ∗ in Figure 13) decomposes into a polymer-rich phase and a polymer-lean phase, the compositions of which are defined by tie lines. If the decomposition takes place in the region between the binodal and spinodal a nucleation and growth mechanism of the polymer-rich and polymer-lean phases dominates, leading to structures undesirable for gas separation. Decomposition below the critical point leads to a dispersion of polymer nodules within the polymer-lean phase; decomposition above the critical point leads to a closed cellular structure of an encapsulated polymer-lean phase. The preferred inversion path is to quickly bring the dope within spinodal envelope, thus generating an interpenetrating network of polymer-lean and polymer-rich phases which vitrify into a finely porous substructure.

The thermodynamic framework for a ternary dope system lies in Flory–Huggins theory and the Gibbs free energy of mixing for a ternary system is given by:

$$\Delta G_{mix} = n_1\phi_1 + n_2\phi_2 + n_3\phi_3 + \chi_{12}n_1\phi_2$$
$$+ \chi_{13}n_1\phi_3 + \chi_{23}n_2\phi_3 \qquad [14]$$

where the subscripts refer to the nonsolvent (1), the solvent (2) and the polymer (3). The notations n_i and ϕ_i are the number of moles and the volume of
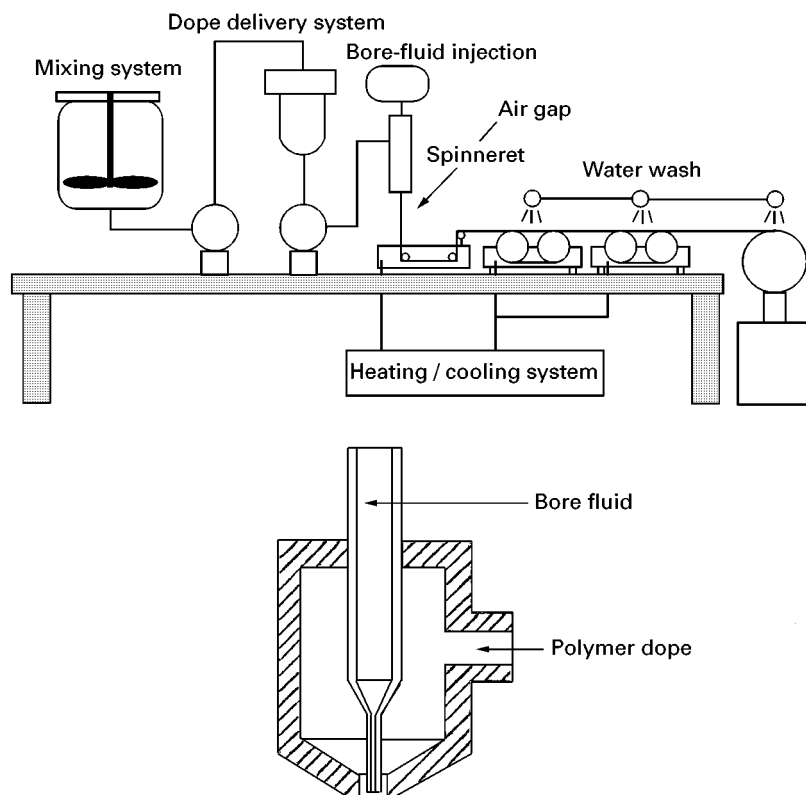

Figure 17 Hollow-fibre membrane spinning apparatus and cross-section of spinnerette.

component i and χ_{ij} is the interaction parameter accounting for the nonideality of the mixture. At equilibrium the chemical potentials (u) of the components in all the phases are equal and are given by eqn [15], which defines the binodal envelope. The composition for the spinodal line is given by the solution to eqn [16], where v_i is the pure component molar volume of species i:

$$\frac{\Delta u_i}{RT} = \frac{\delta}{\delta n_i} \frac{\{\Delta G_{mix}\}}{RT} \qquad [15]$$

$$(1/\phi_1 + v_1/v_2\phi_2 - 2\chi_{12})(1/\phi_1 + v_1/v_3\phi_3 - 2\chi_{13})$$
$$\times (1/\phi_1 + \chi_{23}v_1/v_2 - \chi_{12} - \chi_{13}) = 0 \qquad [16]$$

Composite Membranes

The above discussion also applies to the formation of composite or multilayer membranes. Composite membranes can be categorized as either a dense, isotropic or asymmetric coating of a high performance separating layer on a microporous substrate. Composite membranes are fabricated in two operations, substrate formation followed by dip coating, allowing for the independent optimization of coating and substrate properties. Gas transport through composite membranes is described by the series resistance model by analogy to an electrical circuit. For a two-layer composite consisting of a thin layer of polymer A on a substrate of polymer B, the flux of gas i though the membrane is given by eqn [17], where l is the thickness of the respective layers:

$$J_i = \Delta P(l_B/Po_B + l_A/Po_A) \qquad [17]$$

Regardless of their method of formation a critical element of gas separation membranes is that the skin layer must be as thin as possible in order to produce a high flux membrane. The practical limit to the skin layer thickness is thought to be in the range of 500–1000 Å. Concurrently, the skin layer must be free of manufacturing defects or pinholes. A defective surface area fraction as low as $10^{-5}\%$ can lower selectivity to an extent that the membrane is not suitable for gas separation. Conventional manufacturing processes are not capable of achieving this level of reliability. The second enabling development in commercializing gas separation membrane technology was the demonstration of a poly(dimethylsiloxane) defect repair coating to effectively 'plug' manufacturing pinholes and eliminate bulk flow through the defects (**Figure 14**). Gas permeation through this multicomponent system is described by the series resistance model analogous to an electrical
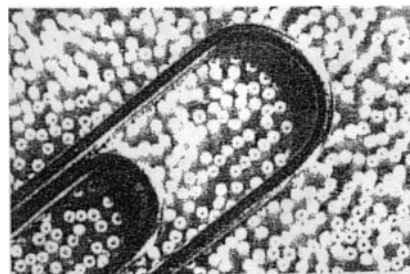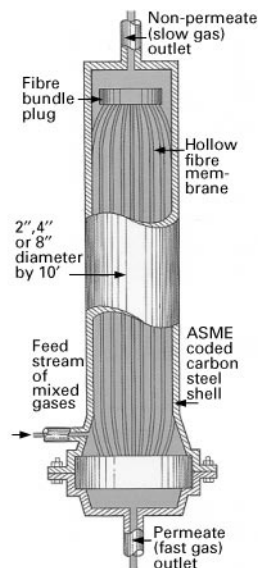

Figure 18   Hollow-fibre membrane element.

circuit. The total resistance is given by the sum resistances in the coating layer (R_c); the parallel resistance in the defective skin layer; ($R_{sk,d}$); and the resistance of the substrate R_{sub}:

$$R_{tot} = R_c + R_{sk,d} + R_{sub}$$

$$= R_c + \frac{R_{sk} \times R_d}{R_{sk} + R_d} + R_{sub} \qquad [18]$$

After repair, the resistance of the defect, R'_d is greater than R_d and also, $R_{sk} > R'_d$, so that the effective permeability of the composite approaches the intrinsic permeability of a defect-free membrane.

Membrane Devices

Gas separation modules can be prepared from flat sheets as plate and frame assemblies and spiral-wound elements. Hollow fibres can be fine fibres ($< 1000 \mu m$ OD) or tubular. In general only fine fibres and spiral-wound elements combine
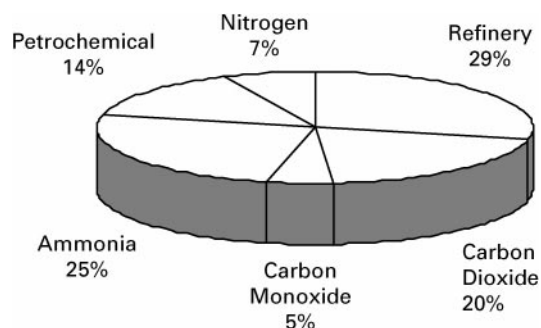
Figure 19 Membrane technology: breakdown by application.

performance and cost parameters providing economic viability. The benefits of the spiral-wound configuration include ease of fabrication and low pressure drop but manufacturing costs are high and the membrane surface area to module volume ratio is low ($\approx 700 \text{ m}^2 \text{ m}^{-3}$), leading to larger, heavier systems. Hollow fibre modules can achieve very high surface area/volume ratio ($> 5000 \text{ m}^2 \text{ m}^{-3}$) and provide a higher degree of countercurrent flow but are more difficult to fabricate and can have high pressure drop.

Flat Sheets and Spiral-Wound Elements

A schematic representation of a flat-sheet asymmetric casting device is shown in **Figure 15**. Flat-sheet membranes are typically produced on a nonwoven cloth which provides support for the nascent membrane. These nonwoven cloths are commercially available on large rolls of 24–48 inches. A thin liquid film of dope solution is metered by a doctor blade onto the nonwoven cloth while the fabric ro-

tates around a stainless steel roller. The nascent membrane is quenched in the gel tank, washed and collected on a take-up roller. A generic spiral-wound element is shown in **Figure 16**. The simplest configuration consists of a central collection pipe around which is wound and glued an envelope of flat-sheet membrane. The envelope contains the membrane and feed and permeate spacer channels. The spacer material is an extremely porous, inert material. Feed gas flows parallel to the permeate pipe; permeating gas flows into the permeate spacer and is collected in the pipe. Higher membrane areas can be achieved using the multileaved method in which two to four sheets of membrane are wrapped simultaneously.

Hollow Fibres

A second asymmetric membrane geometry is that of a hollow fibre. The ultrathin skin is present on the external surface of the fibre. Like the flat sheet, the wall of the fibre is microporous and offers low resistance to gas flow. The permeating gases collect in the bore or lumen of the fibre. A generic hollow-fibre spinning device is shown in **Figure 17**. The apparatus contains a dope reservoir, a bore fluid reservoir, pumps, coagulation baths, wash baths and a take-up winder. The dope solution and bore fluid are co-extruded through a die, resulting in a sheath of polymer around the bore fluid (typically water). This nascent fibre is then coagulated, washed and dried. Hollow-fibre devices contain thousands, even hundreds of thousands, of individual fibres within a single pressure housing (**Figure 18**). The feed gas is usually fed to the outside of the fibre (shell side) although some processes route the feed gas through the fibre

Table 4 Selected membrane applications

| Category	Range of operation	Application	Gases separated
Hydrogen recovery	95% H_2 $<$5 MMSCFD	Ammonia synthesis purge gas Syngas ratio adjustment Hydrotreater off gas	H_2/N_2, Ar H_2/CO
Nitrogen production	95–97% N_2 0.1–2.0 T/D	Inerting: fuel tanks; food transportation Gas and oil drilling	N_2/O_2, CO_2 N_2/O_2, CO_2, H_2O
Oxygen	40% O_2	Oxygen-enriched air	O_2/N_2
Carbon dioxide removal	95 $+$ % CH_4 $<$40 MMSCFD	Natural gas sweetening Enhanced oil recovery Landfill gas	CO_2/CH_4
Dehydration	Dewpoint to $-40°C$	Instrument air Natural gas dehydration	H_2O/air or N_2 H_2O/CH_4
Misc.		Semiconductor process gas	Perfluorocarbon from N_2
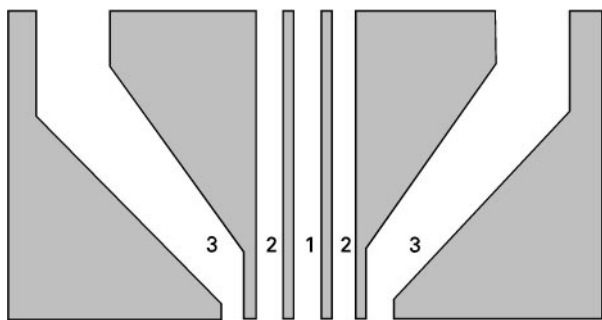
Figure 20 Triple-orifice die for co-extrusion. 1, bore fluid; 2, substrate polymer dope; 3, coating polymer dope.

bore, especially when well-defined flow characteristics are required.

Applications

The first successful commercial activity in gas separation by membranes began in 1977 with the introduction of the Prism® membrane system by Monsanto (now Air Products and Chemicals, Inc.), to recover H_2 from ammonia synthesis plant purge gas. Installed membrane capacity in 1977 was only 5 MMSCFD (million standard cubic feet per day) and grew to over 3500 MMSCFD by 1996. Approximately two-thirds of current installed membrane capacity is used for H_2 separation, which includes ammonia purge gas, refinery and petrochemical applications (**Figure 19**). Significant growth is expected for N_2 and CO_2 separations. While the specifics will vary according to application, a generic membrane system will include a compressor if the source gas is not available at pressure and pretreatment to remove condensible, corrosive or reactive components. The partial listing of applications (**Table 4**) represents established uses for gas separations. Expanding the slate continues to be a focus of membrane manufacturers and research institutes.

Future Trends

The concurrent need for high performance polymers and low cost membranes has resulted in research into hybrid polymer systems and improved manufacturing processes. Four areas currently being explored are:

1. *Polymer blends*: A hybrid polymer system in which expensive, high performance polymers form a continuous phase in a multipolymer blend.

Examples include Matrimid/Ultem® 1000 and aromatic polyimides/polysulfone.

2. *Coextruded composite hollow fibres*: An improved hollow-fibre spinning process in which a forming asymmetric substrate is simultaneously coated with a thin film of separating polymer by employing a die similar to that shown in **Figure 20**. This is a paradigm shift away from separate substrate fabrication and subsequent coating practices. The co-extrusion processes should lower manufacturing costs and relax price constraints on new high performance polymers.

3. *Organic/inorganic mixed matrix membranes*: A nanocomposite composite is a hybrid in which very small particles of a material with high diffusive selectivity such as a microporous carbon is dispersed with an organic polymer matrix. Such materials combine the high selectivity of the inorganic with the processability of the organic polymer matrix.

4. *Computational methods*: Molecular modelling of gas transport through rubbery polymers has already proven successful. Its application to glassy polymers is significantly more difficult, primarily because of the poorly defined nature of the glassy state, but significant progress has been made in the last several years. As our understanding of gas–polymer and polymer–polymer interactions improves and merges with advancing computer technology, widespread use of molecular dynamics should provide significant insight into gas separation with polymer membranes.

Further Reading

Ho WS and Sircar KK (1992) *Membrane Handbook*. New York: Chapman & Hall.

Hwang ST and Kammermeyer K (1975) *Membranes in Separations*. New York: Wiley.

Kesting RE (1985) *Synthetic Polymeric Membranes: A Structural Perspective*, 2nd edn. New York: Wiley.

Koros WJ and Fleming GK (1993) Membrane-based gas separations. *Journal of Membrane Science* 83: 1–80.

Mulder M (1991) *Basic Principles of Membrane Technology*. Dordrecht: Kluwer.

Paul DR and Yampolski YP (eds) (1994) *Polymeric Gas Separation Membranes*. Boca Raton, FL: CRC Press.

Robeson LM (1991) Correlation of separation factor vs. permeability for polymeric membranes. *Journal of Membrane Science* 62: 165.

Stern SA (1994) Polymers for gas separations: the next decade. *J ournal of Membrane Science* 94: 1–65.